Journal of Marine Science and Technology

Volume 22 | Issue 2 Article 14

REPRODUCING LABORATORY-SCALE RIP CURRENTS ON A BARRED BEACH BY A BOUSSINESQ WAVE MODEL

Ke-Zhao Fang
The State Key Laboratory of Coastal and Offshore Engineering, Dalian University of Technology, Dalian City, China.,
kfang@dlut.edu.cn

Ji-Wei Yin
The State Key Laboratory of Coastal and Offshore Engineering, Dalian University of Technology, Dalian City, China.

Zhi-Li Zou
The State Key Laboratory of Coastal and Offshore Engineering, Dalian University of Technology, Dalian City, China.

Zhong-Bo Liu
The State Key Laboratory of Coastal and Offshore Engineering, Dalian University of Technology, Dalian City, China.

Ping Dong
Department of Civil Engineering, University of Dundee, Dundee City, UK

REPRODUCING LABORATORY-SCALE RIP CURRENTS ON A BARRED BEACH BY A BOUSSINESQ WAVE MODEL

Acknowledgements

The authors would like to thank the finical support from National Natural Science Foundation of China under Grant 51009018, Key Laboratory of Coastal Disaster and Defence, Ministry of Education, Hohai University. We also would like to thank Dr. Haas Kelvin for providing the detailed surveyed bathymetry data. The valuable comments from anonymous reviewers are greatly appreciated.

Journal of Marine Science and Technology, Vol. 22, No. 2, pp. 231-239 (2014)
DOI: 10.6119/JMST-013-0509-1

REPRODUCING LABORATORY-SCALE RIP CURRENTS ON A BARRED BEACH BY A BOUSSINESQ WAVE MODEL

Ke-Zhao Fang[1], Ji-Wei Yin[1], Zhi-Li Zou[1], Zhong-Bo Liu[1], and Ping Dong[2]

Key words: Boussinesq wave model, rip current, barred beach, domain effect, mean current.

ABSTRACT

The pioneering work of Haller [8] on physically investigating bathymetry-controlled rip currents in the laboratory is a standard benchmark test for verifying numerical nearshore circulation models. In this paper, a numerical model based on higher-order Boussinesq equations was developed to reproduce the number of experiments involved in such an investigation, with emphasis on the effect of computational domain size on the numerical results. A set of Boussinesq equations with optimum linear properties and second-order full nonlinearity were solved using a higher-order finite difference scheme. Wave breaking, moving shoreline, bottom friction, and mixing were all treated empirically. The developed model was first run to simulate the rip current under full spatial and time-domain conditions. The computed mean quantities, including wave height, mean water level, and mean current, were compared with the experimental data and favorable agreements were found. The effects of computational domain size on the computation results were then investigated by conducting numerical experiments. The Willmott index was introduced to evaluate the agreements between the computed results and data. Inter-comparisons between the computation results and measurements demonstrated that the computational domain size significantly influenced the numerical results. Thus, running a Boussinesq wave model under full spatial and time-domain conditions is recommended to reproduce Haller's experiment.

I. INTRODUCTION

Rip currents, which are shore-normal, rapid, and intense offshore-directed jets of water that originate within the surf zone, greatly influence sediment and pollutant transportation, thereby affecting the coastal morphology and nearshore water quality. Public safety issues are closely linked to intense rip currents, especially in tourist beaches. For example, in the state of Florida, rip currents account for more than 80% of all lifeguard rescue efforts, and more beachgoers fall victim to rip currents than to lighting, hurricanes, and tornadoes. Thus, rip currents are listed as the number one natural hazard in the US [13]. These aforementioned issues illustrate the importance of rip currents and have initiated numerous studies, as reviewed by MacMahan [13] and Darlymple [2].

Among the many published research results available on rip currents, Haller's experimental bathymetry and layout are typical [8]. In the experiments, rip currents generated on a barred beach with two incised channels were investigated. Many scholars have subsequently employed the same bathymetry and layout to investigate bathymetry-controlled rip currents [4, 9, 10, 15], and these physical experiments have greatly contributed to our insights into the complex rip current. Haller's experiments also provide an excellent benchmark test for verifying numerical nearshore circulation models [1, 3, 5-7, 12, 14]. Boussinesq wave models, used by Chen *et al*. [1], Nwogu [14], Lu and Yu [12], and Fang *et al*. [3], can present good predictions after careful tuning of the involved parameters.

Compared with the real space and time scales in Haller's experiments, however, later simulations were conducted with certain simplifications of the computational domain size. The wave basin size in Haller's experiments is 17 m long and 18.2 m wide with a duration of about 27 min. By contrast, Chen *et al*. [1], Lu and Yu [12], and Fang *et al*. [3] only used the top half of the experimental topography and the simulation time was reduced to 200 s. Although Nwogu [14] used the full-size wave basin, the simulation time was also limited to 200 s. Results from the Boussinesq wave model using the full computational domain size have never been reported. The Boussinesq wave model belongs to the phase-resolving type, which describes wave motion in a wave-by-wave manner and requires considerable computation efforts. The aforementioned simplifications on computational domain size are explained in this way.

Paper submitted 12/15/12; revised 01/24/13; accepted 05/09/13. Author for correspondence: Ke-Zhao Fang (e-mail: kfang@dlut.edu.cn).
[1] *The State Key Laboratory of Coastal and Offshore Engineering, Dalian University of Technology, Dalian City, China.*
[2] *Department of Civil Engineering, University of Dundee, Dundee City, UK.*

When using a Boussinesq-type wave model to reproduce Haller's experiments, the following must be considered: (1) the simplifications will inevitably introduce uncertainties to the computation results; (2) compared with three-dimensional (3D) models, the computational cost of a Boussinesq wave model has already been greatly reduced by integration along the water depth; thus, a relatively computation-cheaper model can be used to simulate laboratory-scale rip currents; (3) since fewer domain effects on the physical phenomena are the main advantage of a numerical model, introduction of an extra domain effect when a numerical model is used to reproduce laboratory-scale experiments must be deliberated on; and (4) the extent by which domain reduction affects the numerical results from a Boussinesq wave model has yet to be determined. Previous studies of Boussinesq-type simulations scarcely underline these problems.

The present study addresses the effect of computational domain size on the computation results by conducting numerical experiments. A numerical model based on a set of fully nonlinear Boussinesq equations is first developed to reproduce Haller's experiments under full-domain conditions. Then, the validated model is used to conduct numerical experiments using different spatial and time sizes, and the effects of reducing spatial or time domains on the numerical results are investigated.

II. MODEL DESCRIPTION AND SIMULATION SETTING

1. Boussinesq-type Wave Model

The governing equations used in the present study are the extended version of the second-order fully nonlinear equations of Zou [17]. The two-dimensional (2D) forms of the equations are

$$\beta\eta_t + \nabla\cdot(\Lambda\bar{\boldsymbol{u}}) = f \tag{1}$$

$$\bar{\boldsymbol{u}}_t + (\bar{\boldsymbol{u}}\cdot\nabla)\bar{\boldsymbol{u}} + g\nabla\eta + \boldsymbol{G} = \frac{1}{2}h\nabla[\nabla\cdot(h\bar{\boldsymbol{u}})_t] - \frac{1}{6}h^2\nabla(\nabla\cdot\bar{\boldsymbol{u}}_t)$$
$$+B_1h^2\nabla[\nabla\cdot(\bar{\boldsymbol{u}}_t + g\nabla\eta)] + B_2\nabla[\nabla\cdot(h^2\bar{\boldsymbol{u}}_t + gh^2\nabla\eta)] + \boldsymbol{R} \tag{2}$$

$$\boldsymbol{G} = \nabla\left\{\frac{1}{3}d^2[(\nabla\cdot\bar{\boldsymbol{u}})^2 - \bar{\boldsymbol{u}}\cdot\nabla^2\bar{\boldsymbol{u}} - \frac{1}{10}\nabla^2(\bar{\boldsymbol{u}}\cdot\bar{\boldsymbol{u}})]\right\}$$
$$+\nabla\eta d[\frac{1}{3}(\nabla\cdot\bar{\boldsymbol{u}})^2 - \frac{1}{3}\bar{\boldsymbol{u}}\cdot\nabla^2\bar{\boldsymbol{u}} - \nabla\cdot\bar{\boldsymbol{u}}_t] - \frac{1}{3}\eta(2h+\eta)\nabla^2\bar{\boldsymbol{u}}_t \tag{3}$$

where η is the surface elevation, h is the water depth, $d = h + \eta$ is the local water depth, g is the gravitational acceleration, and $\bar{\boldsymbol{u}}$ is the depth-averaged velocity. The coefficients B_1 and B_2 are set as 29/885 and 2/59, respectively, after optimizing dispersion equations and shoaling properties. The aforementioned equations allow a Pade [2, 2] approximation of the exact dispersion and are applicable in intermediate water. As well, the equations have fully nonlinear characteristics (up to the second order) and can be used to describe the wave motion with strong nonlinearity.

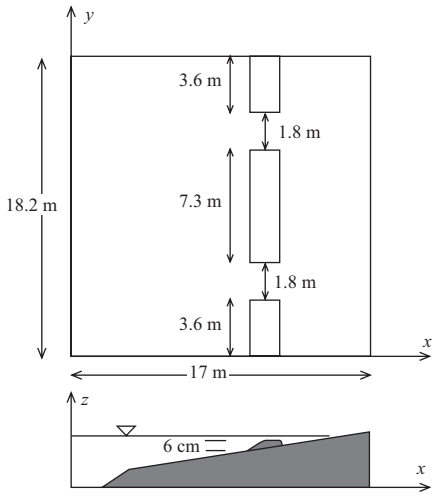

Fig. 1. Sketch of Haller's experiments.

Λ in Eq. (1) accounts for the inclusion of porous beaches to take into the moving shoreline. f on the right-hand size of Eq. (1) is the function for internal wave generation. $\boldsymbol{R}$ in Eq. (2) is defined as $\boldsymbol{R} = \boldsymbol{R}_b + \boldsymbol{R}_f + \boldsymbol{R}_s$, where $\boldsymbol{R}_b$ represents energy dissipation caused by wave breaking (including subgrid mixing), $\boldsymbol{R}_f$ is the bottom friction, and $\boldsymbol{R}_s$ is the sponge layer used to absorb wave energy. All of these terms are identical to those in the FUNWAVE model [1, 11], and readers can refer to that model or that by Fang *et al*. [3].

Two parameters in porous beaches λ and δ, control the shape of the slot and are set as $\lambda = 60$ and $\delta = 0.01$. The bottom friction is set as 0.01 after tuning of the numerical results to match the experimental data. The parameters for eddy viscosity breaking are set to the following values in simulations: wave breaking initiation parameter $\eta_t^I = 0.30\sqrt{gh}$, wave breaking cease parameter $\eta_t^I = 0.05\sqrt{gh}$, transition period $T^* = 5\sqrt{h/g}$, strength of wave breaking δ_b = 1.2, and mixing turbulence parameter C_m = 0.25.

The numerical implementation mainly follows the FUNWAVE model [1, 11]. The numerical procedure consists of solving an algebraic expression for η and tri-diagonal equations for $\bar{\boldsymbol{u}}$ along grid lines at the x and y directions. Details of such may be found in the studies of Fang *et al.* [3].

2. Model Setting

A plan view and a cross section of the wave basin in Haller's experiment are shown in Fig. 1, where the origin is located at the intersection point of the wave maker and one side wall. The wave basin is 17.2 m long, 18.2 m wide, and contains a planar concrete beach of 1:30 slope as well as a

steep (1:5) toe structure. A longshore bar parallel to the wave maker is located between approximately x = 11.1 m and 12.3 m with the bar crest at x = 12.0 m, resulting in a minimum water depth of 0.048 m on the crest. Two gaps of approximately 1.8 m wide, centered at 1/4 and 3/4 of the basin width, are incised to mimic rip channels. The bathymetry was intended to be planar and the two rip channels were intended to be symmetric and equal to each other; however, bathymetric survey data clearly show some differences [8]. A more detailed description of the experiments is provided in [8]. Only the top half of the bathymetry was used for numerical simulations by Chen *et al*. [1], Lu and Yu [12], and Fang *et al.* [3].

The proposed model was run for 27 min and the last half of the data collection period (819 s) was used for mean quantity calculations. These settings are identical to those in Haller's experiment, thus creating a full domain simulation. In the simulation, grid sizes along the y and x directions are 0.10 m and 0.05 cm, respectively, and the time step is 0.01 s. Regular waves 0.048 m high and of 1.0 s periodicity are generated using internal source function at x = 4.0 m, where the water depth is 0.363 m. The entire computational domain is enclosed by solid walls and sponge layers are placed in front of walls near the two ends of the computational domain to absorb reflected waves.

To evaluate the agreements between numerical results and experimental data for a given quantity v, the Willmott index [16] is used. This index is introduced as

$$d_v = 1 - \frac{\sum_{j=1}^{n}\left[y(j)-x(j)\right]^2}{\sum_{j=1}^{n}\left[\left|y(j)-\bar{x}\right|+\left|x(j)-\bar{x}\right|\right]^2} \qquad (4)$$

where $x(j)$ is the measured data point, $y(j)$ is the computation result, and $\bar{x}$ is the mean value of series $y(j)$. Perfect agreement is indicated by d_v = 1, whereas d_v = 0 indicates complete disagreement.

III. NUMERICAL RESULTS FROM THE FULL DOMAIN SIMULATION

Numerical results are presented and compared with the experimental data in this section. The quantities compared include mean wave height (H), mean water level (MWL), mean cross-shore current (U), longshore current (V), and mean flow field. As the measurements from the experiments cover most areas of wave basins, their comparison with the computation results will reasonably show the overall performance of the numerical model on reproducing the experiments.

1. Wave Height and Mean Water Level

The computed wave heights, plotted in Fig. 2, show good

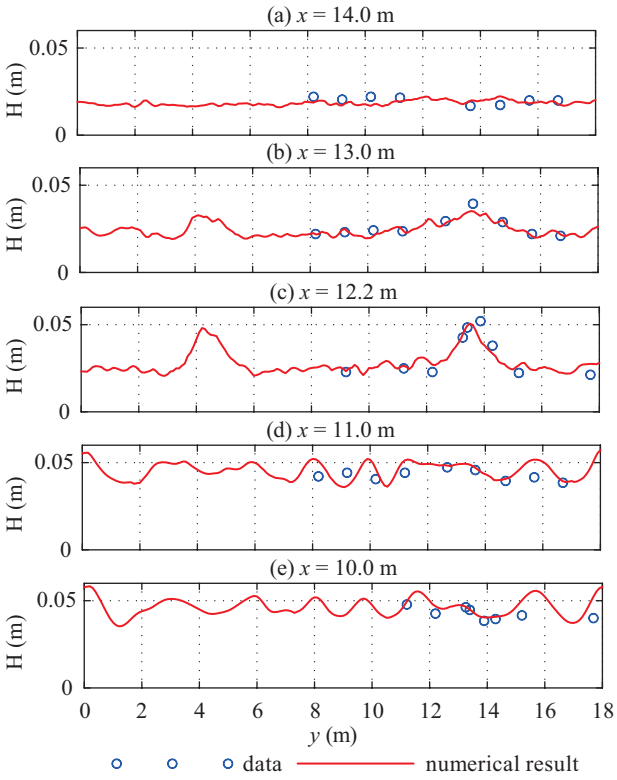

Fig. 2. Comparison of time-averaged computed wave heights with experimental data.

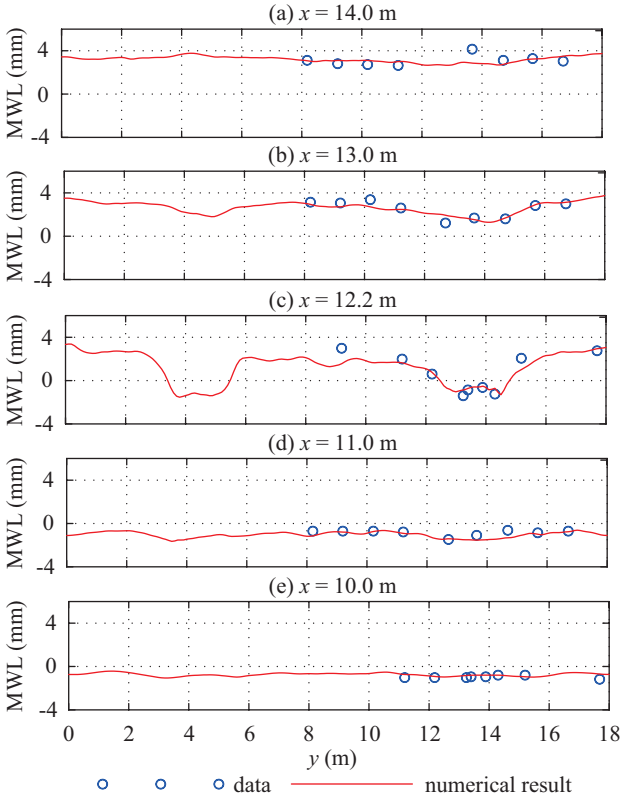

Fig. 3. Comparison of time-averaged computed mean water levels with experimental data.

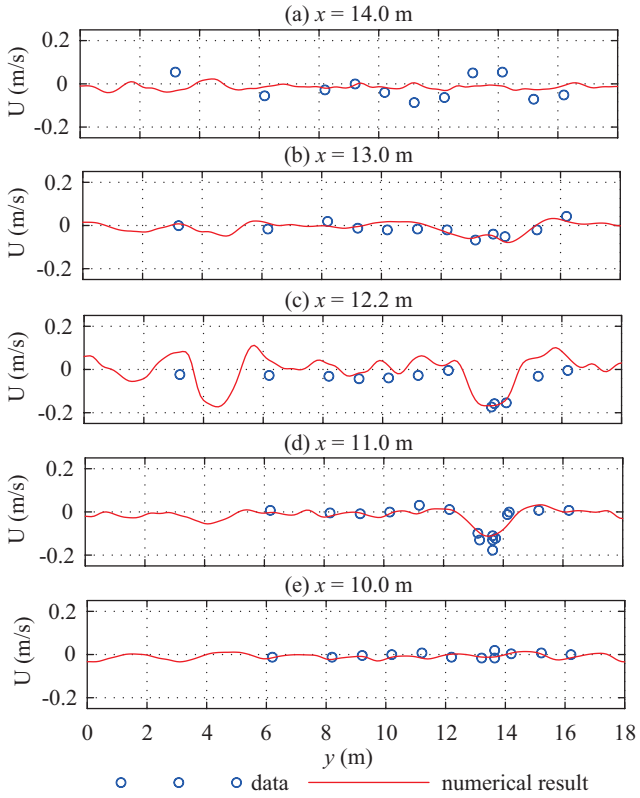

Fig. 4. Comparison of time-averaged computed cross-shore currents with experimental data.

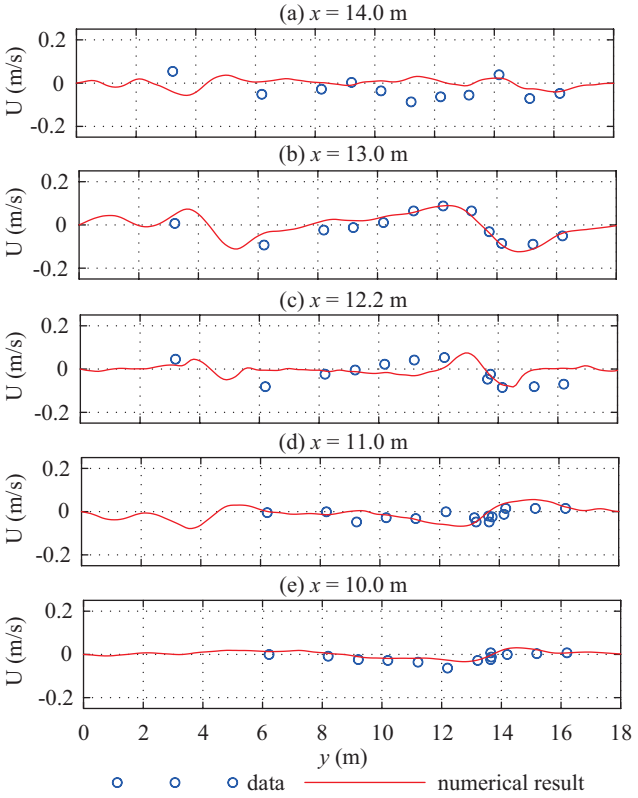

Fig. 5. Comparison of time-averaged computed long-shore currents with experimental data.

agreement with the experimental data. The increase in wave height because of the shoaling process and decrease in wave height after wave breaking are well predicted from relatively deep water (x = 10.0 m) to shoreline (x = 14.0 m). Particularly, the delayed wave breaking in the rip channel is also well reproduced. The value of d_H computed from Eq. (4) for the wave height turns out to be 0.915, which demonstrates that the present wave model is reasonable.

The computed mean water level ($\overline{\eta}$), shown in Fig. 3, show good agreement with the experimental data except for some underestimates at x = 12.2 m and x = 13.0 m. Before wave breaking, the mean water level has a negative value at x = 10.0 m and x = 11.0 m, which indicates a setdown. After wave breaking occurs, the mean water level begins to increase to a positive value and the maximum value is reached near the shoreline (x = 14.0 m). The wave setup in the barred region is higher than that in the rip channel, which will induce a longshore pressure gradient, finally driving the current to converge and flow out from in the rip channel to form a rip current. The index agreement for mean water level $d_{\overline{\eta}}$ is 0.936. The high values of d_H and $d_{\overline{\eta}}$ denote that the variations in surface elevations are well captured by the numerical model.

2. Time-Averaged Current

The computation results for cross-shore mean current (U) and longshore mean current (V) are presented in Figs. 4 and 5, respectively. The corresponding values of d_U and d_V computed from Eq. (4) are 0.844 and 0.755, respectively. These two relatively lower values are mainly caused by the discrepancy near the shoreline region x = 14.0 m, as shown in the figures. The main features of rip currents are well reproduced. The offshore-directed currents, i.e., rip currents, are obvious in the rip channel at x = 11.2 m and x = 11.0 m. At farther offshore positions, such as x = 10.0 m, rip currents are dissipated because of the mixing mechanism. The rip feeder is also clearly shown in Fig. 5, where the longshore mean currents at the two sides of the rip channel have opposite signs, indicating that these currents flow in the opposite direction to converge in the rip channel. The asymmetry of mean currents is also demonstrated; such asymmetry is mainly due to longshore non-uniformities of the bathymetry and consistent with observations of experiments and numerical results from a quasi 3D model [6].

Fig. 6 shows more detailed comparisons of the cross-shore current in the rip channel along three longshore sections at x = 11.5, 11.8, and 12 m. The model accurately captures the amplitude, width, and longshore variations in the rip current and shows excellent agreement with the experimental data. The index of agreement for the cross-shore current is fairly high, with d_U = 0.955. This high value shows some attractive aspects of the numerical model, since the mean current in the

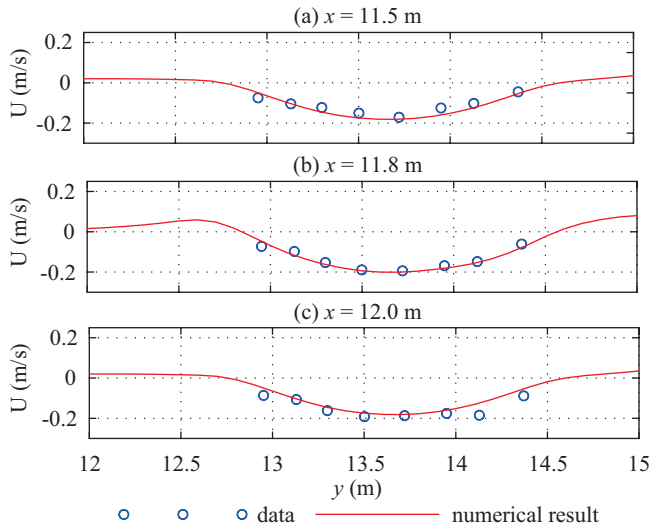

Fig. 6. Comparison of time-averaged computed cross-shore currents in the channel with experimental data.

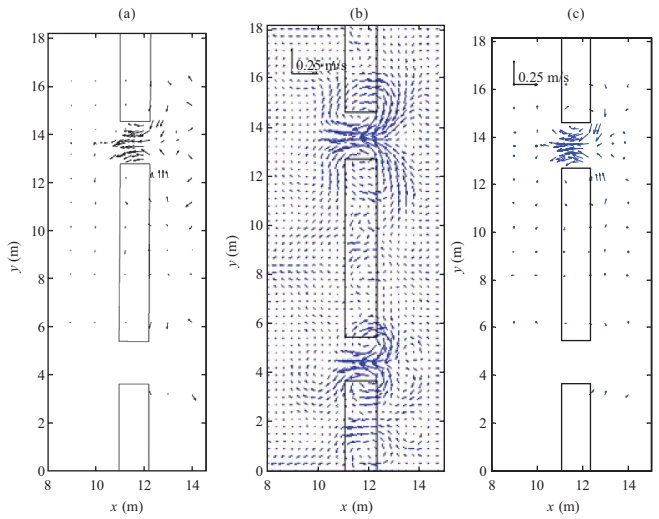

Fig. 7. Time-averaged below-trough velocity from the experimental data (left panel), the simulation (middle panel), and the simulation at the same points as the experimental data (the third panel).

channel is always the strongest current. Accurate prediction of the maximum rip current is extremely crucial for lifeguards or coastal engineers.

3. Mean Current Field

The depth-integrated current from the model is displayed in Fig. 7 and compared with the experimental data. The experimental data shown here are obtained from many repeated runs of the experiment with identical wave conditions but different measuring locations [8]. The classical flow pattern of rip currents, *i.e.*, rip feeder, rip neck, and rip head, are well reproduced by the model and appear similar to the measured flow field. The slight basin center biased rip header, which is shown by the measurements, is also reproduced by the model. To facilitate comparisons between the model results and data, currents from the model obtained only at locations where the measurements were made are shown in the third panel of Fig. 7. The figure shows that the recirculation cells close to the shoreline have similar dimensions and that the flow along the offshore edge of the central bar is parallel to the shore. The flow patterns in the top and down channels are not identical, which is mainly due to the slight non-uniformities of the bathymetry. No measurements in Haller's [8] experiments quantitatively support this difference but this asymmetry was also observed. Further analysis of the asymmetry will be presented in the following section using experimental data from Test R in the experiments of Haas *et al.* [4], which is designed to supplement the experiments of Haller [8].

4. Mean Current Field and Movement of Vorticity

Besides the time-averaged quantities listed above for comparison, some interesting instantaneous phenomena are also observed in the experiments. The first is the slow plural of the rip current during its offshore-directed motion and the second is the asymmetry of the rip current in the top and bottom rip channels. Research has shown that irregularities in the actual bathymetry are responsible for variations in rip behavior [6] and that the slow plural is due to the instability of rip currents [6, 8]. Further investigations with respect to these two aspects will be made to demonstrate model's ability in capturing these time-varying characteristics.

Four snapshots of computed vorticity and velocity are shown in Fig. 8, where the quantities are obtained by averaging a series of recorders every two periods. The unstable features of rip currents may be observed from the figures. The vorticity and velocity fields develop fully in the channel and propagate offshore but the rip continually meanders from side to side and attenuates in the process of moving toward deep-water regions. The aforementioned asymmetry between the upper and lower channels may also be observed in the figure, where the vorticity and velocity fields are asymmetric. The scale and intensity of the mean current originating from the upper channel are stronger than those from the lower channel. A similar trend is also observed for long time-averaged current fields (Fig. 7).

Fig. 9 shows the low-pass filtered time series of cross-shore velocity from the measurements of Haas *et al*. [4] and present simulations offshore of the edge of the top (x = 10.8 m, y = 13.6 m) and lower (x = 10.8 m, y = 4.6 m) channels. The measurements show significant differences in the frequency or magnitude of the rip events between two locations. The simulation presents a similar trend, *i.e.*, rip events in the top channel occur more frequently and with more strength than those in the bottom channel. Although some distinct differences may be observed in the time series, the measured and long-time averaged velocities are similar. Both measurements and simulation show that the rip current only occurs sporadically.

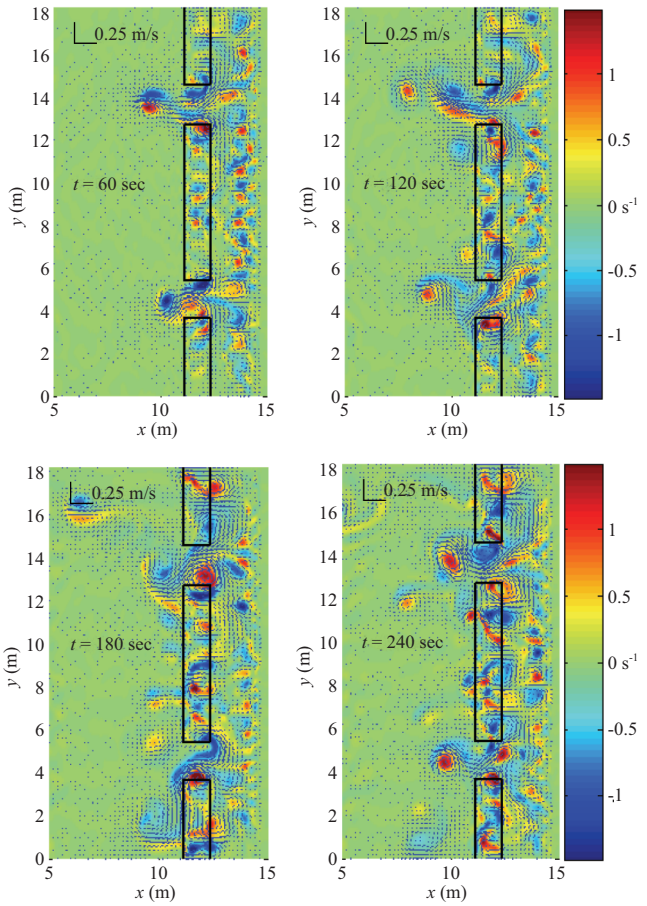

Fig. 8. Four instantaneous snapshots of simulated vorticity and velocity vectors.

The numerical simulation shown above illustrates that the present model can capture the main features of the slow plural of rip currents as well as the difference between two rip channels. However, distinct differences may also be found. The time series shown in Fig. 9 denotes the limited ability of the Boussinesq model in accurately reproducing the temporal variability of rip currents. This limitation is acceptable, considering the following aspects. First, expecting the present 2D numerical model to capture the complete details of a complex 3D process is unrealistic. Second, the main mechanisms that dominate nearshore circulation, such as wave breaking, bottom friction, and turbulence mixing, are only treated by ad-hoc methods in the Boussinesq model.

IV. NEMERICAL EXPERIMENTS

The numerical results from the full domain simulation in Section III demonstrate that the present model predicts the spatial variability of the wave-induced nearshore circulation well and captures the main features of temporal variability. Thus, we can confidently run the model using different spatial and time domains to reach reliable numerical results.

Table 1. Spatial and temporal scale for four cases.

	case 1	case 2	case 3	case 4
Computational domain	full	full	half	half
Simulation time	27 min	200 s	27 min	200 s

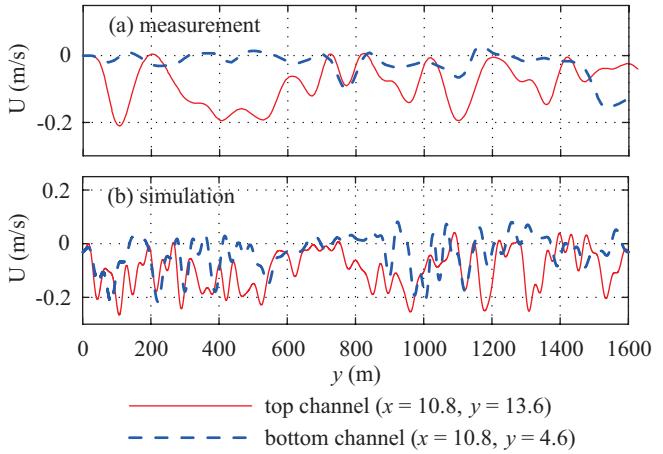

Fig. 9. Low-pass filter time series of the cross-shore velocity of rip currents at x = 10.8 m, y =13.6 m (solid line) and y = 4.6 (dashed line) from (a) the measurements of Haas *et al.* [7] and (b) the simulation.

1. Case Settings

Four cases with different spatial and temporal scales are set for numerical experiments, as shown in Table 1. Case 1: full bathymetry and duration (27 min), which has been completed in Section III; Case 2: the bathymetry is identical to that in case 1 but the simulation time is reduced to 200 s, which is significantly shorter than that in case 1; Case 3: half the size of the full bathymetry and the simulation time is 27 min; and Case 4: half the size of the full bathymetry and the simulation time is 200 s. Except for the spatial and time scales, all of the remaining parameters and conditions are identical to those in case 1. The simulation times for cases 2 and 4 are typical values used by previous studies [1, 3, 12, 14]. The time series used for computing mean quantities is 819 s for cases 1 and 3, whereas the averaging period for cases 2 and 4 begins approximately at the time the first wave arrives at the shoreline and ends at the completion of the simulation [1].

2. Comparison of Wilmott Index for Mean Quantities

The Willmott indices of wave height, MWL, U, V, and mean cross-shore current in the channel determined from the four cases are summarized in Table 2.

The value of d_H for case 1 is 0.915, which is significantly higher than those in other cases, indicating better agreement with the experimental data. By contrast, case 4 presents a minimum index value of 0.815, denoting relatively poor prediction ability. The computed Willmott indices of MWL for the four cases are almost identical, indicating that good agreement is obtained for all cases.

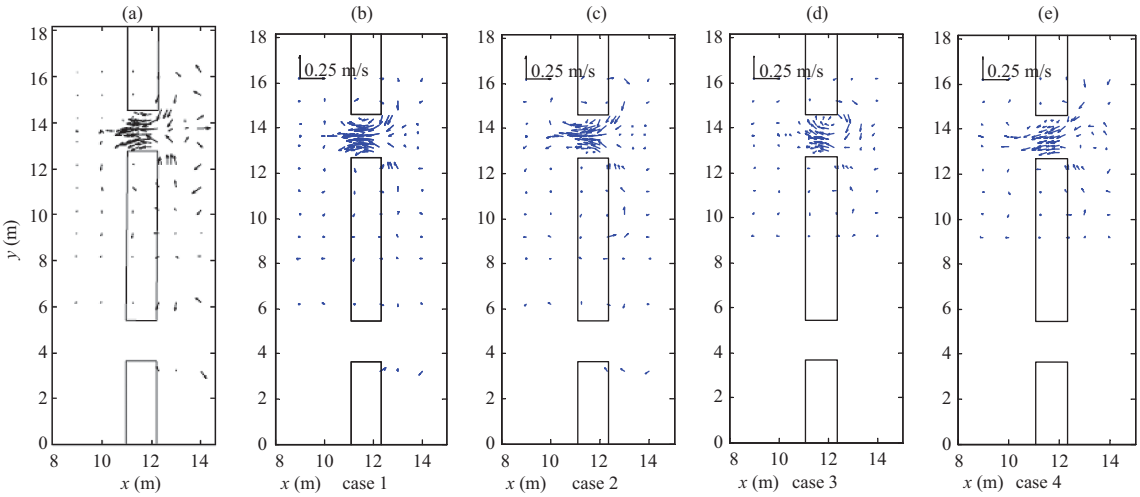

Fig. 11. Time-averaged velocity vectors obtained from (a) the experimental data and from (b) case 1, (c) case 2, (d) case 3, and (e) case 4.

Table 2. A summary of the index of agreement for quantities from four cases.

case	H	WML	U	V	U (in channel)
case 1	0.915	0.936	0.844	0.755	0.955
case 2	0.893	0.961	0.816	0.739	0.819
case 3	0.866	0.944	0.632	0.629	0.733
case 4	0.815	0.963	0.833	0.838	0.806

From the aforementioned comparisons, we can conclude that simulations using full domains present optimal numerical results whereas simulations using reduced spatial or time scales present relatively poor predictions. To fully capture the differences among these four cases, the profile of the mean cross-shore current in the rip channel and mean current field will be further investigated.

From the aforementioned comparisons, we can conclude that simulations using full domains present optimal numerical results whereas simulations using reduced spatial or time scales present relatively poor predictions. To fully capture the differences among these four cases, the profile of the mean cross-shore current in the rip channel and mean current field will be further investigated.

3. Mean Cross-shore Current in Channel and Mean Current field

The numerical results of rip currents in the channel from four cases are plotted in Fig. 10 and compared with the experimental data. Case 1 accurately presents both the amplitude and the distribution of the mean current whereas case 3 gives the poorest predictions by underestimating the strength of rip currents and distorting its distribution in the rip channel. Cases 2 and 4 overestimate the amplitude of rip currents and the predicted mean flows are strongly biased.

The time-averaged velocity vectors from four cases are shown in Fig. 11; those from Haller's experiment are also shown as a reference. Cases 3 and 4 fail to provide flow information of the bottom half wave basin because only the top half of the bathymetry was used. Comparing the four vector diagrams with the experimental data, we can see that cases 1 and 2 predict almost the same flow pattern. However, as Fig. 11 shows, case 2 actually presents the wrong profile in the rip channel. Case 3 only gives the local mean current in the rip channel and fails to predict the offshore-directed rip head. Case 4 presents a significantly biased mean flow and the amplitude of the mean current is greatly underestimated.

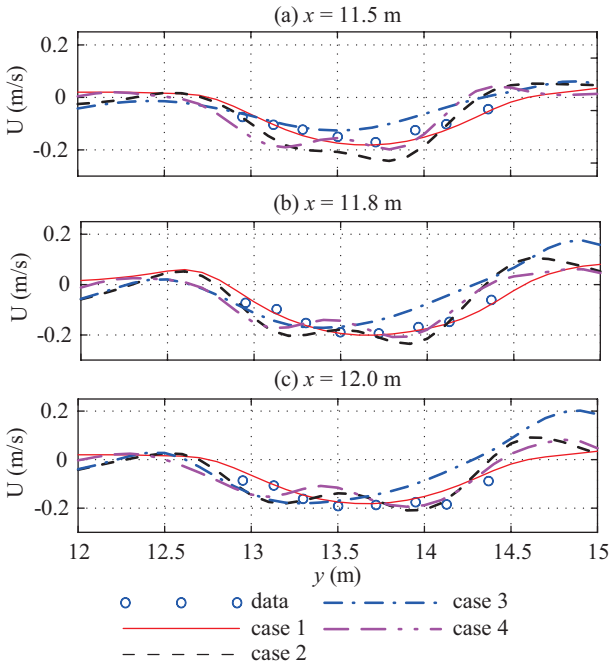

Fig. 10. Comparison of computed time-averaged cross-shore current in the channel from four cases with experimental data.

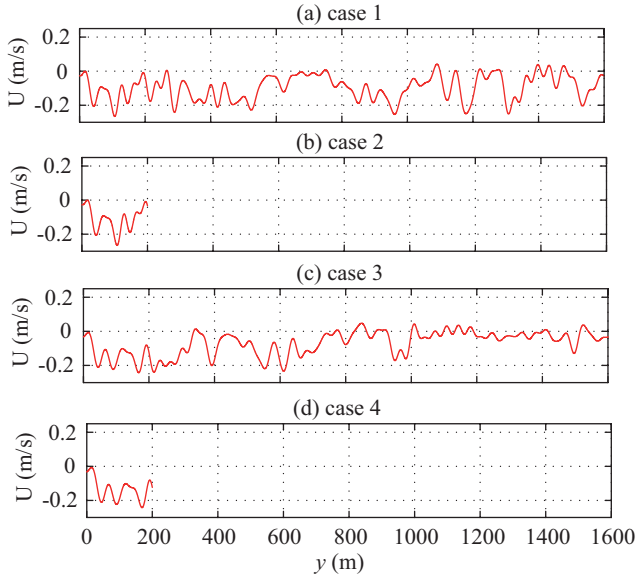

Fig. 12. Comparison of computed and low-pass filtered time series of the cross-shore velocity in the rip current at x = 10.8 m and y = 13.6 m.

4. Further Analysis and Discussion of Domain Effects on Numerical Results

The aforementioned comparisons show that the computational domain greatly influences the numerical results. For the spatial domain, using the top half of the wave basin implies complete symmetry of the actual bathymetry or, in the very least, that irregularities can be ignored. Both our numerical experiments and those of Haas *et al*. [6] show that variations in the bathymetry cannot be ignored and that they significantly change the flow patterns between two rips. Long-term simulation results obtained from using the top half of the basin are also physically incorrect as they predict a solid wall in the centerline where the water region should be, thereby decreasing the simulation accuracy, as shown in case 3.

The computational duration effect on the numerical results is further investigated by comparing the low-pass filtered time series of cross-shore currents at the offshore edge of the top channel (x = 10.8 m, y = 13.6 m), as shown in Fig. 12. It is interesting to see that all of the time series have an initial offshore-directed flow event near the beginning of simulation, which is due to drainage from the initial surge of water shoreward when waves begin [6]. If only the first 200 s is used for simulation, the time-averaged quantity U would be almost identical for all four cases because of the initial surge event. However, this result is not accurate, as shown in the previous sections. Only long-term simulation can remove the effects of the initial surge event, yielding results more representative of the real rip current. The experimental investigation of Haas *et al*. [4] revealed this phenomenon, where all time series of measured velocities (Figs. 6, 7, 13, and 14 in [4]) showed almost identical initial surge events but long-term averages resulted in apparently different quantities. That also may be the reason why Haas *et al*. [6] simulated Haller's experiment using full spatial and time domains. Relatively high indices of agreement are found for cases 2 and 4 in Table 2, which we believe are not completely reliable based on the aforementioned analysis.

V. CONCLUSION

Domain effects on the numerical results when using a Boussinesq-type wave model to reproduce Haller's experiments are investigated in the present paper by conducting numerical experiments. A 2D wave-breaking model based on fully nonlinear Boussinesq-type equations is first developed to reproduce the experiment of Haller. Numerical results, including wave height, mean water level, mean longshore, and cross-shore current, from the full-scale simulations agree well with the experiments. Differences in mean current field in the two rip channels and the transient rip current and vorticity movement, which have been observed in previous experiments, are also well reproduced by the full-scale simulation. The overall performance of the present model illustrates its ability to reproduce wave breaking-induced nearshore circulation.

The effects of different spatial and time scales adopted in the simulation on the computation results are then investigated by conducting numerical experiments for four cases using different spatial and time scales. The Willmott index evaluates the agreement between the numerical results and experimental data. Detailed comparisons between the numerical results and experimental data demonstrate that the scales significantly influence the computation results and that the full-scale simulation presents the best numerical results and has superior performance compared with simulations using reduced spatial or time scales. Using only the top half of the wave basin is not advisable as variations in the actual bathymetry are ignored and long-term simulations are not supported. To run the Boussinesq model for short times is incorrect as the initial surge of rip current dominates the initial stage of the flow pattern. Thus, to reproduce Haller's experiments using a Boussinesq-type wave model, conducting simulations under full-scale conditions, which is believed to be consistent with the intrinsic "phase resolving" nature of the model, is recommended by the authors.

ACKNOWLEDGMENTS

The authors would like to thank the finical support from National Natural Science Foundation of China under Grant 51009018, Key Laboratory of Coastal Disaster and Defence, Ministry of Education, Hohai University. We also would like to thank Dr. Haas Kelvin for providing the detailed surveyed bathymetry data. The valuable comments from anonymous reviewers are greatly appreciated.

REFERENCES

1. Chen, Q., Dalrymple, R. A., Kirby, J. T., Kennedy, A. B., and Haller, M. C., "Boussinesq modeling of a rip current system," *Journal of Geophysical Research*, Vol. 104, No. C9, pp. 20617-20637 (1999).
2. Dalrymple, R. A., MacMahan, J. H., Reniers, Ad J. H. M., and Nelko, V., "Rip current," *Annual Review of Fluid Mechanics*, Vol. 43, pp. 551-581 (2011).
3. Fang, K. Z., Zou, Z. L., and Liu, Z. B., "Numerical simulation of rip current generated on a barred beach," *Chinese Journal of Hydrodynamics*, Vol. 24, No. 4, pp. 314-320 (2011).
4. Haas, K. A. and Svendsen, I. A., "Laboratory measurements of the vertical structure of rip current," *Journal of Geophysical Research*, Vol. 107, No. C5, pp. 1-19 (2002).
5. Haas, K. A. and Svendsen, I. A., "3-D modeling of rip current," *The Twenty-Seventh International Conference on Coastal Engineering*, Vol. 108, No. C7, pp. 1-15 (2001).
6. Haas, K. A., Svendsen, I. A., Haller, M. C., and Zhao, Q., "Quasi-three-dimensional modeling of rip current systems," *Journal of Geophysical Research*, Vol. 108, No. C7, pp. 1-21 (2003).
7. Haas, K. A. and Warne, J. C., "Comparing a quasi-3D to a full 3D nearshore circulation model: SHORECIRC and ROMS," *Ocean Modelling*, Vol. 26, Nos. 1-2, pp. 91-103 (2009).
8. Haller, M. C., *Rip Current Dynamics and Nearshore Circulation*, Doctor Dissertation, University of Delaware, USA (1999).
9. He, L., *Video-Based Particle Image Velocimetry of Laboratory Rip Current*, Thesis, University of Delaware, USA (2006).
10. Kennedy, A. B., Zhang, Y., and Haas, K. A., "Rip current with varying gap widths," *Journal of Waterway, Port, Coastal, and Ocean Engineering*, Vol. 134, No. 1, pp. 61-65 (2008).
11. Kirby, J. T., Wei, G., Chen, Q., Kennedy, A. B., and Dalrymple, R. A., "FUNWAVE 1.0 Fully nonlinear Boussinesq wave model documentation and user's manual," Research Report, CACR-98-06, Newwark (1998).
12. Lu, J. and Yu, X. P., "Model for both nearshore waves and wave-induced current based on Boussinesq equations," *Chinese Journal of Hydrodynamics*, Vol. 23, No. 3, pp. 314-320 (2008).
13. MacMahan, J. H., Thornton, Ed. B., and Reniers, Ad J. H. M, "Rip current review," *Coastal Engineering*, Vol. 53, pp. 191-208 (2006).
14. Nwogu, O. K., "Numerical prediction of rip current on barred beaches," *Proceedings of the 4th International Symposium on Ocean Wave Measurement and Analysis*, San Francisco, USA, pp. 1396-1405 (2001).
15. Sapp, B. K., *Observations of Laboratory Rip Current*, Thesis, Georgia Institute of Technology, USA (2006).
16. Willmott, C. J., "On the validation of models," *Physical Geography*, Vol. 2, pp. 184-194 (1981).
17. Zou, Z. L., "Higher order Boussinesq equations," *Ocean Engineering*, Vol. 26, pp. 767-792 (1999).